### Metallic Nanowires

Synthesis of Ultrathin Palladium and Platinum Nanowires and a Study of Their Magnetic Properties**

Xiaowei Teng, Wei-Qiang Han, Wei Ku, and Markus Hücker*

Careful control of the size, shape, and composition allows the properties of various noble metals, particularly palladium and platinum, to be varied, which leads to a wide range of applications for these metals in fields such as catalysis and magnetism.[1,2] In confined nanoscale systems such as ultrathin nanowires or nanoclusters, which are often only a few atoms thick, the reduced degree of coordination and bonding favors more localized electronic states as well as narrower bands and larger densities of states, which often lead to rather exotic magnetic behavior.[3] Several 4d and 5d noble metals such as Pd, Pt, and Au have been shown experimentally to be ferromagnetic in two-dimensional (2D) atomic layers[4–6] or zero-dimensional (0D) nanoclusters,[7–12] whereas their bulk counterparts are diamagnetic or paramagnetic. Although theoretical studies have predicted that a one-dimensional (1D) nanowire should show different magnetic properties from a 0D nanocluster,[13,14] no experimental confirmation has yet been reported for the magnetism of 1D nanowires of 4d or 5d metals, mainly because of the limited number of synthetic approaches to monodisperse ultrathin nanowires.

Herein we report the synthesis of ultrathin Pd and Pt nanowires by a modified phase-transfer method in which inorganic palladium nitride or platinum chloride is transferred into a mixture of octadecylamine (ODA) and toluene using a new type of phase-transfer agent, namely *n*-dodecyltrimethylammonium bromide (DTAB).[15,16] Subsequent addition of a large excess of the reducing agent sodium tetrahydroborate ($NaBH_4$) in aqueous solution reduces the palladium or platinum cations rapidly to form thermodynamically unstable elongated primary nanostructures (PNs). Secondary growth of these PNs apparently takes place in preferred equivalent directions and also along ⟨111⟩, which leads to the growth of thread-like quasi-nanowires (Scheme 1).

Figure 1 shows transmission electron microscopy (TEM) images of these thread-like Pd and Pt nanowires. The width of the Pd and Pt nanowires is 2.4 ± 0.2 and 2.3 ± 0.2 nm, respectively, and their length is over 30 nm. The high-
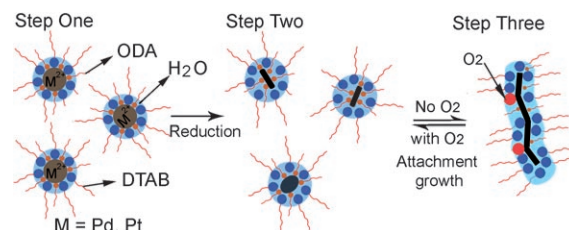
Scheme 1. Formation of Pd and Pt nanowires.

resolution TEM images (Figures 1b and 1d) show that both nanowires are polycrystalline with well-defined lattice planes; both twinning boundaries and stacking faults are also observed. The lattice spacings of 2.7 and 2.8 Å can be assigned to the {111} planes of Pd and Pt, respectively. X-ray diffraction measurements show that both nanowires belong to the *Fm3m* space group.[17]

Crystal structure anisotropy is believed to be the main driving force for the anisotropic growth of nanostructures.[18] However, this 1D growth of Pt and Pd is rather unexpected owing to their symmetric cubic lattices. HRTEM reveals that each nanowire is composed of several single-crystalline, elongated PNs. Similar PN-to-wire transformations have already been observed for the oriented growth of different types of nanocrystals.[19] Unlike quantum dots, however, where the dipole moment is the driving force, the oriented attachment in these Pd and Pt nanostructures is most likely due to the specific binding of a capping agent to certain crystal surfaces. In general, the shape of nanomaterials is highly dependent on the competitive growth rate along the low index crystal planes in the presence of surfactants.[18a] Bases, for example, seem to preferentially adsorb on the {100} surfaces of Pd and Pt and facilitate the growth of PNs along the ⟨111⟩ directions.[20]

Our results show that the oxygen content is critical to nanowire formation. Since the PNs are interconnected at various angles, twin boundaries and stacking faults are readily observed along the nanowires. These defects are the primary sites for oxygen absorption and remain susceptible to oxidative etching.[21] Elongated nanoparticles (ENP) 3.5 ± 0.8 nm wide and 5–25 nm long were formed after two hours in an oxidative etching experiment upon exposure to air; nearly spherical nanoparticles 27 ± 4.3 (Pd) and 31 ± 3.9 nm (Pt) in diameter were formed after 12 h (Figures 1 g,h). We believe that the dissolved oxygen inhibits the secondary growth of PNs by oxidatively etching the nanowires at the twin boundary defects. Subsequent Ostwald ripening accounts for the shape evolution from ENPs to nearly spherical nanoparticles.

[*] Dr. X. Teng, Dr. W.-Q. Han
Center for Functional Nanomaterials
Brookhaven National Laboratory,
Upton, NY 11973 (USA)
Fax: (+1) 631-344-3093
E-mail: whan@bnl.gov

Dr. W. Ku, Dr. M. Hücker
Condensed Matter Physics & Materials Science Department
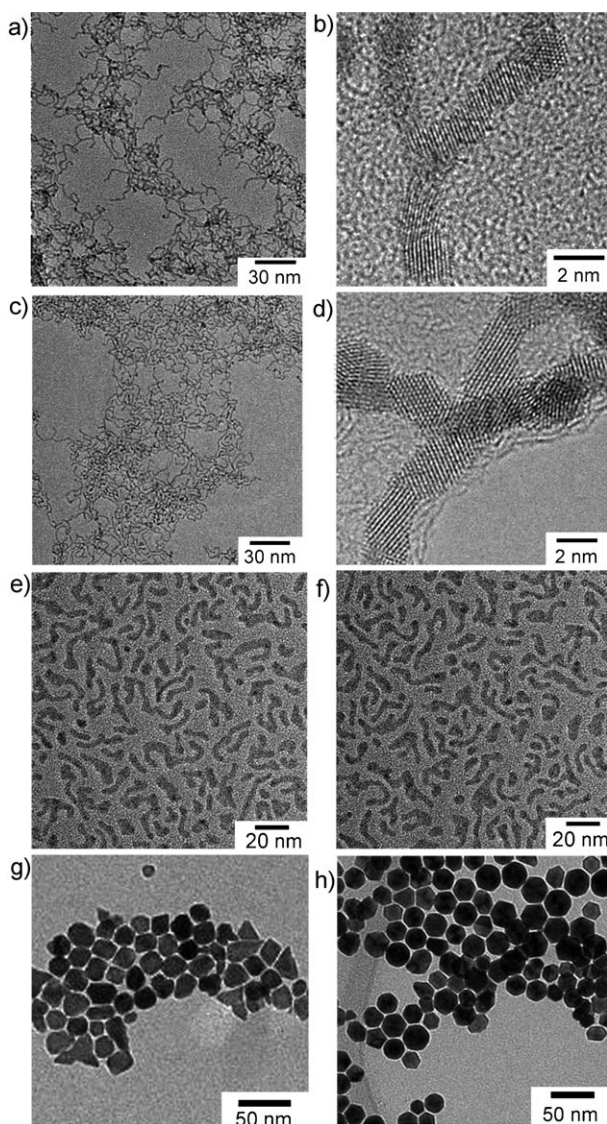Brookhaven National Laboratory, Upton, NY 11973 (USA)

Figure 1. TEM images of as-synthesized Pd (a) and Pt (c) nanowires and their high-resolution TEM images (b and d, respectively). TEM images of the Pd (e) and Pt (f) elongated nanoparticles (ENP) obtained after 2 h in air and the nearly spherical Pd (g) and Pt (h) nanoparticles obtained after 12 h.

Figure 2. a) Temperature-dependent magnetization of Pd (black) and Pt (red) nanowires obtained by zero-field cooling in an external field of 1000 Oe. b–d) Field-dependence of the magnetization of Pd and Pt nanowires at 5 (b), 300 (c), and 2 K (d). e,f) The coercivity (H_C) and biased field (H_B) of Pd (e) and Pt (f) nanowires as a function of temperature.

SQUID magnetometry measurements revealed a strong temperature-dependent magnetization in the as-synthesized nanowires (Figure 2 a). The magnetizations are roughly constant above a temperature of about 60 K for Pt and 30 K for Pd nanowires, whereas below those temperatures the magnetizations increase sharply. This steep increase of the magnetization at low temperatures is similar to the behavior of stabilizer-capped Au and Pt nanoparticles and is mainly due to the temperature-independent Pauli-paramagnetic parts of the magnetization in the low-temperature range.[9,11] The low magnetic moments observed indicate that the overall ferromagnetism of the wire is suppressed significantly, as in the bulk form of these material, owing to the enhanced itinerancy associated with the macroscopic length scale of the wires. The nature of the adsorbed capping agents might also account for the change of magnetic moment. For example, when nano-
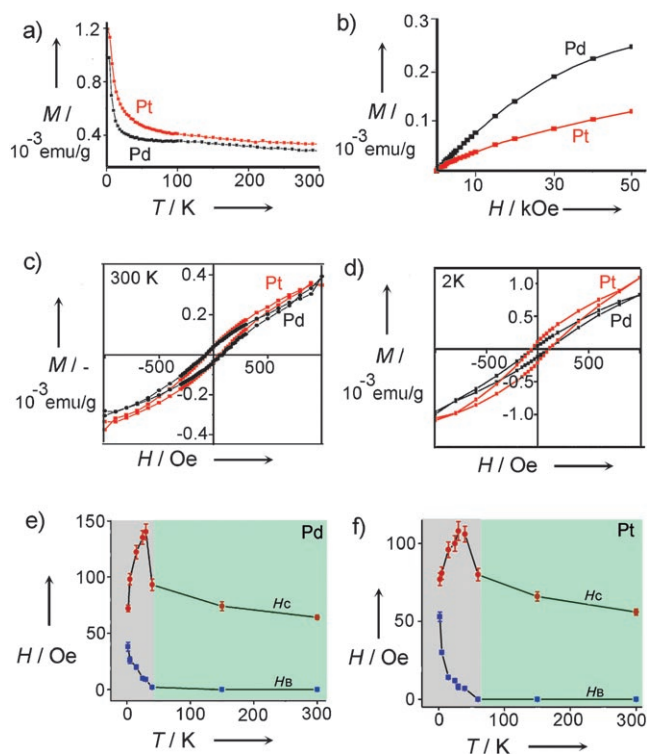
materials are stabilized by covalent bonds to thiol-derivatized alkenes or adsorbed oxygen, the increase in the density of holes localized by the bonded S and O atoms might give rise to the ferromagnetism, whereas there are no covalent bonds between the metal core and the protective surfactant in alkylamine-protected nanomaterials, therefore less ferromagnetic order might be expected.[8,22]

The magnetization curves of Pd and Pt nanowires in an applied field of up to 50 kOe (5 T) are shown in Figure 2 b and the coercivity (H_C) in the hysteresis loop at 300 K can be seen in Figure 2 c. These combined results suggest that both nanowires are ferromagnetic rather than superparamagnetic. A similar unsaturated magnetization at high field has been reported for Pd nanoparticles, thereby indicating the presence of adsorbed molecules on the surface.[8]

A remarkable "magnetic memory" effect is observed for these nanowires at low temperatures. Thus, instead of a hysteresis loop with regular symmetry, the loop exhibits a distinct shift that is biased in the direction of the cooling field and which remains even after removing the field. These loops show that H_B, the shift of the hysteresis loop along the field's axis, emerges at about 40 K for the Pd nanowires and at about 60 K for the Pt nanowires. The value of H_B increases rapidly at lower temperatures up to 40 ± 4 Oe for Pd and 53 ± 3 Oe for Pt at 2 K (Figures 2 e,f).

We propose a microscopic model whereby the memory effect observed in nanowires is a consequence of magneto-

elastic coupling. In the course of field cooling the local magnetic moments become aligned by the strong field. This alignment is associated with a relaxation of the local lattice that is coupled to the magnetic moment. As illustrated in Figure 3 some of the "vulnerable" local lattice structure (e.g.,
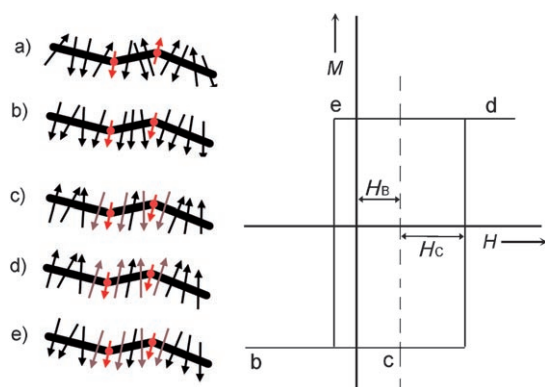

Figure 3. Moment configuration at different stages in a shifted hysteresis loop. a) Random regular moments (black arrow) and "localized" moments (red arrow) seen at "vulnerable" lattice structures (red spot) in the nanowire without a magnetic field; b) all moments (black and red arrows) are aligned after cooling to a certain temperature in the presence of a field; c) the regular moments (black arrow) rotate in the opposite direction and the localized moments remain "locked" when the field is reversed. Some moments (purple arrow) align preferentially in the direction of adjacent "locked" moments (red arrow) due to interfacial interactions. In other words, "locked" moments exert a microscopic torque on the adjacent moments; d) an extra field (H_B) is needed to overcome the microscopic torque and completely reverse the moments (both black and purple arrows); e) when the field returns to its original direction, the aligned moments are reversed in the smaller field (H_C-H_B) because the "localized" moments exert a torque in the same direction as the field.

twin boundaries, stacking faults along the nanowires) become "locked" into a *meta*-stable configuration when various phonon modes are removed upon cooling. These locked "defect spots" fix the corresponding local magnetic moments even after reversing the external field and thereby create a bias in the neighboring moments in the direction of the field during cooling. This magneto-elastic effect should persist until the temperature is high enough to create a large number of phonon modes that can release the "locked" local lattice structure. We presume that the higher bias onset temperature of Pt compared with that of Pd reflects its heavier atomic mass, which modifies the phonon properties to a greater extent.

While it is not possible to unambiguously identify the origin of the magnetism from our experimental analysis, the very small moment observed suggests that the magnetic moment resides primarily in "defects" in the structure, such as twinning boundaries and stacking faults, as well as changes of "boundary conditions" such as twists and bending of the wire. Local magnetic instability near these defects is enhanced by the collapse of the density of states resulting from localization of the electrons, which is a necessary condition considering the lack of itinerant magnetism in the bulk form of these

materials. However, because of the long length of these wires, the large number of atoms in this system stabilizes the ferromagnetism and, in particular, the memory effect, and uniquely distinguishes the long wires from ENPs and nearly spherical nanoparticles.

Besides the memory effect mentioned above, the observed coercivity shows an unusual temperature dependence that is contrary to that of typical itinerant ferromagnetic materials: it becomes weaker at lower temperature (Figure 2 e,f) regardless of the significant enhancement of the magnetic moment. This result strongly suggests an enhanced electron localization in these systems at low temperature, which enhances the local magnetic moment and decreases the ferromagnetic exchange interactions between them. This effect again illustrates the uniqueness of wires (or ensembles of nanoparticles) in the field of nanomagnetism and deserves further scientific investigation.

In summary, we have presented the synthesis of Pd and Pt nanowires with widths of less than 2.5 nm and lengths of over 30 nm. Both nanowires are ferromagnetic up to room temperature, although with unusual shifts in the hysteresis loop at low temperature, instead of being paramagnetic as their bulk forms. A microscopic model suggests that this shift is a consequence of magneto-elastic coupling. We consider that these nanomaterials are an ideal model for studying the magnetism of quasi-1D nanomaterials and also offer opportunities for designing nanodevices with memory-effect-related spintronics.

Experimental Section

All solvents were degassed by bubbling argon through them for at least ten minutes before use. A mixture of $Pd(NO_3)_2$ (Alfa Aesar, 99.95%; 13 mg, 0.06 mmol) or $PtCl_2$ (Alfa Aesar, 99.9%; 16 mg, 0.06 mmol), ODA (Aldrich, 97%; 0.4 g, 1.5 mmol), and DTAB (Aldrich, 98%; 60 mg, 0.2 mmol) was dissolved in toluene (7 mL) by sonicating for 20 min under argon. Reduction was then performed by the dropwise addition of a freshly prepared solution of $NaBH_4$ (Alfa Aesar, 99%; 13 mg, 0.34 mmol) in 2 mL of distilled water. Stirring was stopped after one hour and then distilled water (2 mL) and chloroform (2 mL) were added to the solution. The aqueous solution was discarded and the organic phase containing the alkylamine-stabilized Pt or Pd nanowires was collected. Further separation was conducted by adding ethanol (10 mL) and centrifuging the mixture at 8000 rpm for 10 min. The supernatant was discarded and the collected precipitate was redispersed in chloroform. This process was repeated three times using ethanol and chloroform alternately.

The Pd and Pt ENPs and nearly spherical nanoparticles were synthesized in a similar manner except that air was bubbled through the solvent and the reaction was left open to the air. ENPs and nearly spherical nanoparticles were obtained after 2 and 12 h, respectively.

High-resolution electron microscopy was performed with a field-emission JEM 3000FEG equipped with an energy-dispersive X-ray spectrometry (EDS). The magnetic measurements were conducted on a Superconducting Quantum Interference Device (SQUID; model: MPMS XL Quantum Design). Diamagnetic contributions due to the sample holder were measured previously and removed from the total magnetization. The hysteresis loop was measured in a field-cooled process with a field of −1000 Oe. The temperature-dependent magnetization was measured following the standard zero field cooled (ZFC) procedure in which the sample is cooled from 300 K to 5 K without a field and then heated to 300 K in a field of 1000 Oe. XRD spectra were obtained with a Philips diffractometer equipped

Communications

with a $Cu_{K\alpha}$ X-ray source ($\lambda = 1.5405$ Å) using a step size of 0.02° $2\theta\,s^{-1}$ and 15 seconds per step.

Various measurements were conducted to exclude the possibility that the observed behavior is due to the presence of ferromagnetic impurities. No metal impurities were found in any of the nanowires by energy dispersive X-ray spectrometry analysis, and the SQUID data showed ferromagnetism without loop shifting in the Pd and Pt ENPs, paramagnetism in the nearly spherical nanoparticles, and diamagnetism in the Pd and Pt precursors ($Pd(NO_3)_2$ and $PtCl_2$). A similar magnetic response would be observed for the all these materials if an impurity played a role in their magnetic behavior,.

[1] A. Wieckoweski, E. R. Savinova, E. G. Vayenas in *Catalysis and Electrocatalysis at Nanoparticle Surfaces*, Marcel Dekker, New York, **2000**.

[2] R. C. O'Handley in *Modern Magnetic Materials: Principles and Applications*, Wiley, New York, **2003**.

[3] T. Taniyama, E. Ohta, T. Sato, *Europhys. Lett.* **1997**, *38*, 195–200.

[4] M. J. Zhu, D. M. Bylander, L. Kleinman, *Phys. Rev. B* **1990**, *42*, 2874–2877.

[5] S. Blügel, *Phys. Rev. Lett.* **1992**, *68*, 851–854.

[6] S. Blügel, *Phys. Rev. B* **1995**, *51*, 2025–2028.

[7] B. Sampedro, P. Crespo, A. Hernando, R. Litran, J. C. Sánchez-López, C. López-Cartes, A. Fernandez, J. Ramírez, J. González-Calbet, M. Vallet-Regi, *Phys. Rev. Lett.* **2003**, *91*, 237203.

[8] T. Shinohara, T. Sato, T. Taniyama, *Phys. Rev. Lett.* **2003**, *91*, 197201.

[9] Y. Yamamoto, T. Miura, M. Suzuki, N. Kawamura, H. Miyagawa, T. Nakamura, K. Kobayashi, T. Teranishi, H. Hori, *Phys. Rev. Lett.* **2004**, *93*, 116801.

[10] H. Hori, Y. Yamamoto, T. Iwamoto, T. Miura, T. Teranishi, M. Miyake, *Phys. Rev. B* **2004**, *69*, 174411.

[11] M. A. García, M. L. Ruiz-González, G. F. de La Fuente, P. Crespo, J. M. González, J. Llopis, J. M. González-Calbet, M. Vallet-Regi, A. Hernando, *Chem. Mater.* **2007**, *19*, 889–893.

[12] X. Liu, M. Bauer, H. Bertagnolli, E. Roduner, J. Slageren, F. Phillipp, *Phys. Rev. Lett.* **2006**, *97*, 253401.

[13] N. Zabala, M. J. Puska, R. M. Nieminen, *Phys. Rev. Lett.* **1998**, *80*, 3336–3339.

[14] A. Delin, E. Tosatti, R. Weht, *Phys. Rev. Lett.* **2004**, *92*, 057201.

[15] M. Brust, M. Walker, D. Bethell, D. J. Schiffrin, R. J. Whyman, *J. Chem. Soc. Chem. Commun.* **1994**, 801–802.

[16] K. Wikander, C. Petit, K. Holmberg, M. P. Pileni, *Langmuir* **2006**, *22*, 4863–4868.

[17] Powder Diffraction File (International Centre for Diffraction Data, Newtown Square, PA, **1994**).

[18] a) Z. L. Wang, *J. Phys. Chem. B* **2000**, *104*, 1153–1175; b) Y. N. Xia, P. D. Yang, Y. G. Sun, Y. Y. Wu, B. Mayers, B. Gates, Y. D. Yin, F. Kim, Y. Q. Yan, *Adv. Mater.* **2003**, *15*, 353–389; c) Y. N. Xia, N. J. Halas, *MRS Bull.* **2005**, *30*, 338–344; d) J. Y. Chen, B. J. Wiley, Y. N. Xia, *Langmuir* **2007**, *23*, 4120–4129.

[19] a) R. L. Penn, J. F. Banfield, *Science* **1998**, *281*, 969–971; b) A. P. Alivisatos, *Science* **2000**, *289*, 736–737; c) Z. Y. Tang, N. A. Kotov, M. Giersig, *Science* **2002**, *297*, 237–240; d) Z. Y. Tang, N. A. Kotov, *Adv. Mater.* **2005**, *17*, 951–962.

[20] a) X. W. Teng, H. Yang, *Nano Lett.* **2005**, *5*, 885–891; b) S. Maksimuk, X. W. Teng, H. Yang, *Phys. Chem. Chem. Phys.* **2006**, *8*, 4660–4663; c) X. W. Teng, S. Maksimuk, S. Frommer, H. Yang, *Chem. Mater.* **2007**, *19*, 36–41.

[21] Y. Xiong, J. M. McLellan, Y. D. Yin, Y. N. Xia, *Angew. Chem.* **2007**, *119*, 804–808; *Angew. Chem. Int. Ed.* **2007**, *46*, 790–794.

[22] R. Litrán, B. Sampedro, T. C. Rojas, M. Multigner, J. C. Sánchez-López, P. Crespo, C. López-Cartes, M. A. García, A. Hernando, A. Fernández, *Phys. Rev. B* **2006**, *73*, 054404.